




Calibrating analytical ultracentrifuges

Huaying Zhao¹ · Ai Nguyen¹ · Samuel C. To¹ · Peter Schuck¹ 

Received: 1 October 2020 / Revised: 9 November 2020 / Accepted: 24 November 2020 / Published online: 4 January 2021
© This is a U.S. Government work and not under copyright protection in the US; foreign copyright protection may apply 2021

Abstract

Analytical ultracentrifugation (AUC) is based on the concept of recording and analyzing macroscopic macromolecular redistribution that results from a centrifugal force acting on the mass of suspended macromolecules in solution. Since AUC rests on first principles, it can provide an absolute measurement of macromolecular mass, sedimentation and diffusion coefficients, and many other quantities, provided that the solvent density and viscosity are known, and provided that the instrument is properly calibrated. Unfortunately, a large benchmark study revealed that many instruments exhibit very significant systematic errors. This includes the magnification of the optical detection system used to determine migration distance, the measurement of sedimentation time, and the measurement of the solution temperature governing viscosity. We have previously developed reference materials, tools, and protocols to detect and correct for systematic measurement errors in the AUC by comparison with independently calibrated standards. This ‘external calibration’ resulted in greatly improved precision and consistency of parameters across laboratories. Here we detail the steps required for calibration of the different data dimensions in the AUC. We demonstrate the calibration of three different instruments with absorbance and interference optical detection, and use measurements of the sedimentation coefficient of NISTmAb monomer as a test of consistency. Whereas the measured uncorrected sedimentation coefficients span a wide range from 6.22 to 6.61 S, proper calibration resulted in a tenfold reduced standard deviation of sedimentation coefficients. The calibrated relative standard deviation and mean error of 0.2% and 0.07%, respectively, is comparable with statistical errors and side-by-side repeatability in a single instrument.

Keywords Analytical ultracentrifugation · Instrument calibration · Sedimentation velocity · Stokes radius

Introduction

Analytical ultracentrifugation (AUC) is a classical technique for measuring the hydrodynamic and thermodynamic properties of a variety of particles across a very large size scale, starting from small molecules, to biomacromolecules, such as proteins, nucleic acids, or carbohydrates, as well as synthetic polymers, nanoparticles, supramolecular structures, and entire organisms. Its fundamental principle is the application of a precisely known centrifugal force that acts on

the mass of dissolved particles and causes their directional bias in Brownian motion, which can be assessed by optically measuring the macroscopic redistribution of particles in the solution (Svedberg and Pedersen 1940; Schuck et al. 2015). Since it is label-free, requires no matrix other than solvent, and is directly rooted in first principles, it can make absolute measurements and occupies a unique place among the biophysical techniques. In recent decades, sedimentation velocity (SV)—essentially the dynamic measurement of free fall of particles in the gravitational field—has become the most popular mode of AUC, in part because it can report on the sample size distribution with high hydrodynamic resolution and measure very precisely species’ sedimentation coefficients (Schuck 2013, 2016). The latter informs on, for example, protein solution conformations, and can be used as a sensitive measure of even transient macromolecular interactions (Harding and Rowe 2010; Schuck and Zhao 2017).

The trust placed in the accuracy of AUC requires that all parameter dimensions are correctly calibrated. In principle, for measurement of macromolecular sedimentation velocity,

Special Issue: COST Action CA15126, MOBIEU: Between atom and cell.

✉ Peter Schuck
schuckp@mail.nih.gov

¹ Dynamics of Macromolecular Assembly Section, Laboratory of Cellular Imaging and Macromolecular Biophysics, National Institute of Biomedical Imaging and Bioengineering, National Institutes of Health, Bethesda, MD, USA

the most critical quantities are the rotor rotation frequency generating the centrifugal field, the optical magnification of the detection system for measuring macromolecular migration, the time associated with observed migration, and the rotor temperature governing the solvent viscosity and thereby setting the resistance to migration. The measurement of all of these quantities needs to be examined to validate the accuracy of macromolecular sedimentation parameters. Jointly with 67 laboratories around the world, we have tested the performance of AUC instruments in a benchmark study involving 129 data sets which were collected on the same reference sample (Zhao et al. 2015). We have shown that if calibration errors (i.e., residual errors that occur after carrying out standard calibration procedures provided by the manufacturer) in the critical parameters are left unaccounted for, the sedimentation coefficient of the molecule of interest varies significantly in different instruments, leading to systematic errors of up to 15% and higher, which unfortunately render many quantitative aspects of SV meaningless. This range of values is two orders of magnitude larger than side-by-side repeatability of sedimentation experiments in the same instrument and same run (Errington and Rowe 2003). This highlights the importance of absolute calibration methods that rely on independent ('external') standards that can be traced to SI units.

We have investigated the origin of systematic errors in detail. First, the measurement of the rotation frequency can be accomplished very precisely with access to an electronic timing signal, and we found insignificant discrepancies between nominal and measured values in pilot experiments (Ghirlando et al. 2013). By contrast, the seemingly trivial task of measuring the time between the scans—on the order of minutes or hours—was shockingly found to be in error in 2013 by approximately ~10% (Zhao et al. 2013). Subsequent 'fixes' on the instruments by the manufacturer have reduced but not eliminated this error, with a range of remaining timing errors reported between 0.1 and 2%, depending on scan settings, rotor speed, and instrument (Ghirlando et al. 2013). A very simple and effective strategy to circumvent and essentially eliminate this error is to take the time intervals from metadata of the scan files stored by the operating system (Zhao et al. 2013). This can be conveniently accomplished in the freeware software SEDFIT (sedfitsedphat.nibib.nih.gov/software) or REDATE (kindly provided by Dr. Chad Brautigam at utsouthwestern.edu/labs/mbr/software).

Second, it has been known for many decades that measurement of the temperature of the spinning rotor in a high vacuum is far from trivial and is error-prone (Cecil and Ogston 1948). We have recently revisited this problem by taking advantage of current semiconductor technology, which allows us to quasi-continuously record and store thermistor-based temperature measurements in an inexpensive miniaturized chip and battery assembly, called 'iButton'. It

offers a high temperature resolution and can be calibrated to a NIST-traceable reference thermometer. It can operate in vacuum and be placed on top of the resting rotor. Since it may be exposed to gentle centrifugal forces, it can also be inserted into centrifugal cell assemblies for low-speed experiments, or even be installed onto the axis of a spinning rotor in high-speed experiments (Ghirlando et al. 2013, 2014; Zhao et al. 2014). When using the same nominal setpoint of 20 °C, variation of the real rotor temperature among 67 instruments was found to be > 4 °C, corresponding to differences of water viscosity spanning > 10%, with sedimentation coefficients being proportionally affected. In our experience, run-to-run variation in individual instruments is usually < 0.1 °C, and instrumental deviations of the true temperature setpoint are therefore not stochastic but systematic and will usually persist virtually indefinitely or until the instrument is physically altered. This means that this error would not be detectable in a laboratory with a single instrument.

Finally, the optical detection system measuring the spatial migration introduces potential errors in the distance from the center of rotation and in the measurement of the distance traveled by macromolecules. The former affects the centrifugal field $\sim \omega^2 r$ (where ω is the rotor angular velocity and r the distance from the center of rotation). For example, absolute radial errors of ~0.1 mm in comparison to the average sample distance of $r = 70$ mm would result in about 0.15% error in the g-force. This is significant but close to statistical error and repeatability of the measurement of sedimentation coefficients (Errington and Rowe 2003; Schuck et al. 2015). However, the accuracy of the optical magnification across the ~10 mm sample solution is much more consequential. In the multilaboratory study, instrument errors in optical magnification were generally found on the order of 2%, but with several outliers, some of which in error as much as 15% or more. To solve these problems, we have developed experimental and computational tools (Ghirlando et al. 2013; Zhao et al. 2013, 2014, 2015; LeBrun et al. 2018) to establish proper calibration for the AUC instrument on scan time, temperature, and radial magnification. This is achieved by measurement of external standards and calculating correction factors that account for differences between apparent and true values. Only after all the calibration factors are being accounted for simultaneously, an optimal consistency of the different AUC instruments can be reached. In the multi-laboratory benchmark study, this is highlighted by a five- to tenfold reduction in error for the sedimentation coefficient of a reference molecule in the control experiment (Zhao et al. 2015).

The significance of the systematic errors for AUC highlights the need to carry out such additional control experiments on a stable reference molecule with a well-known s -value. Comparison of the true value with the measured

value after external calibration corrections can provide confidence in accurate data acquisition and instrument performance, or flag the presence of remaining problems. In the previous multilaboratory benchmark study, bovine serum albumin (BSA) was used for this purpose, as it is suitable for long-term storage and can be easily resuspended in situ after SV experiments. Since then, the NISTmAb has become available as a formulated reference molecule from the National Institutes of Standards and Technology (NIST), RM 8671 (Schiel et al. 2018). Thus, it can serve as a more satisfactory reference, as it side-steps possible subtle variation among lots or vendors.

The following protocol reviews the strategies and steps required for the practical implementation of AUC calibration and reference experiments. The complete calibration for AUC contains three components for the data dimensions of time, temperature, and radial magnification, and a validation experiment to test internal consistency. A comprehensive in-depth discussion of theoretical and experimental considerations can be found in Chapter 6 of the book “Basic Principles of AUC” (Schuck et al. 2015), and somewhat more detailed step-by-step instructions can be found in (Zhao et al. 2020). We describe the results of such calibration of three instruments in our laboratory, each with absorbance and Rayleigh interference optical detection, and the results from control experiments using NISTmAb as a reference.

Protocol

Temperature measurement

This requires the iButton temperature logger DS1922L (Maxim Integrated) with NIST-traceable temperature calibration; the latter may be purchased with the iButton or calibration may be carried out using a reference thermometer (Ghirlando et al. 2013). There are different strategies for applying the iButton to AUC measurements, and we will describe the one that does not require a custom-made rotor hole insert (Ghirlando et al. 2013), or modified rotor handle (Zhao et al. 2014), but instead can be carried out without any additional hardware by placing the iButton in a specific way on top of a resting rotor (Ghirlando et al. 2014).

Step 1: Set up the iButton temperature logger

Thermodata viewer software and USB-based iButton adapters are installed in a PC (preferably not the AUC instrument computer). After inserting the iButton into the adapter, it can be programmed to acquire temperature data in 11-bit resolution with a time interval of 1 or 2 min. Start the temperature data acquisition and mark the time.

Step 2: Temperature measurement using a resting rotor.

Insert a standard counterbalance in an An-50 or An-60 TI rotor, and place the rotor into the rotor chamber such that the radiometer at the bottom of the rotor chamber is maximally covered by the metal of the rotor. Place the iButton loosely at the center on top of the counterbalance, with the sensor side down (Fig. 1). Do not install any optical system. Close the rotor chamber, activate the vacuum pump, and adjust the nominal temperature setpoint to 20.0 °C on the instrument console. After a vacuum below 1000 micron is established, enter a run speed of 0 rpm, press the ‘Start’ button (this step is necessary for systems with oil diffusion pumps, but can be carried out for any system). During the following hour, the AUC console will show a temperature reading that slowly approaches the set point. However, additional temperature gradients may persist within the rotor, and therefore additional time is required for temperature equilibration and stabilization. After 3–4 h, stop the run, open the rotor chamber, and retrieve the iButton.

Step 3: Retrieve the temperature data.

Connect the iButton to the computer with thermodata viewer software and export the temperature log. After initial fluctuations and slow equilibration, a steady-state value will have been attained at a time prior to opening the rotor chamber, followed by fluctuations associated with the opening of the rotor chamber and iButton removal. The steady-state value prior to the opening of the chamber reports on the ‘true’



Fig. 1 Picture of iButton positioned top of the counterbalance in an 8-hole rotor for determining the temperature of a resting rotor. Reproduced from (Ghirlando et al. 2014)

rotor temperature corresponding to the AUC temperature setpoint of nominal 20.0 °C.

Step 4: Calculate the temperature calibration factor.

In addition to knowing the true temperature at nominal 20 °C, it is convenient to determine a multiplicative correction factor for *s*-values to reference to the conventional 20 °C standard. This can be achieved by calculating the ratio of solvent viscosity at the true temperature and 20 °C. In case that the desired run temperature differs significantly from 20 °C, the same steps described above should be repeated for that temperature.

Calibration of radial magnification

The manufacturer's instrument radial calibration is based on two reference edges in the counterbalance. Unfortunately, the counterbalance inserts can come loose or be oriented incorrectly, and in some instruments radial calibration can be subject to significant error of unexplained origin (Zhao et al. 2015). Furthermore, this two-point calibration lacks information on linearity of radius measurement.

To achieve independent multi-point calibration with an external standard, we originally used a precision steel mask (Ghirlando et al. 2013). More recently, in collaboration with the US National Institute of Standards and Technology (NIST), we have developed a lithographically patterned window that will be calibrated at NIST against the SI reference, and be available as a Standard Reference Material (SRM) (LeBrun et al. 2018). This is accompanied by a supporting radial calibration software MARC (sedfitsedphat.nibib.nih.gov/software). The unique patterning of the calibration window provides a larger number of radial positions leading to a better and more detailed assessment for radial magnification errors (Fig. 2). The dual pattern allows for correction for rotational misalignment of the mask. In the following, we focus on the use of the SRM calibration window.

The calibration measurement is carried out in a SV run in parallel with the measurement of the sedimentation of the reference molecule. It requires preparation of the radial calibration cell assembly in the following steps:

Step 1: Assemble the reference cell components.

Use a regular cell housing barrel to assemble a standard 12 mm pathlength cell assembly with standard components using a sapphire window as the bottom window, and the calibration window as the top window. Insert the calibration window such that the lithographic pattern faces the centerpiece. Aim to rotate the window such that the

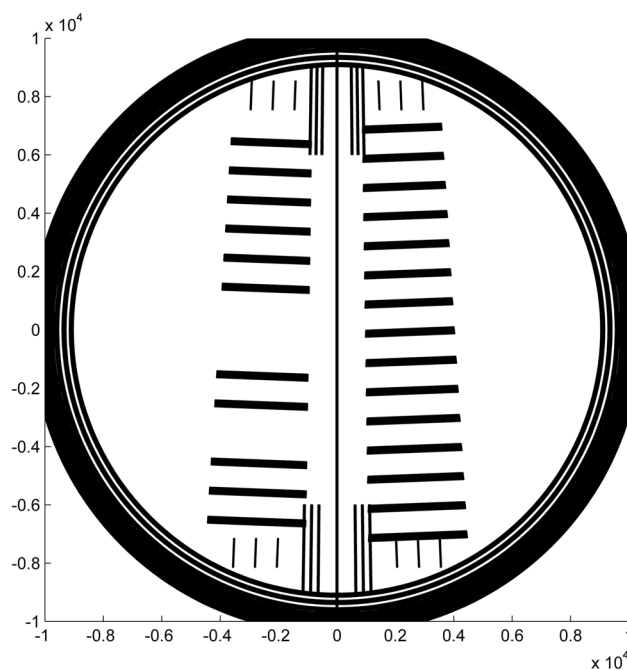


Fig. 2 Calibration pattern on the radial calibration window, in units of μm . The series of lines on the sample and reference side has a pitch of 1 mm, but are shifted by half the pitch. Reproduced from (LeBrun et al. 2018)

center line of symmetry is in parallel with the centerpiece sector divider (the precise rotation will be measured later). Assemble and torque as usual, fill with 450 μL water on both sides and close the fill ports.

Place this cell into any rotor hole but not opposite the counterbalance. Use an extra water-filled cell assembly to achieve weight balance in the opposite rotor hole. Align the rotation of the cell assemblies by matching the scribe marks on the barrel and the rotor.

Step 2: Acquire scan data for the radial reference cell.

For the calibration run, create a data acquisition 'Method' file that includes both scan data acquisition for the radial reference cell, side-by-side with that for the reference molecule (below) sedimenting in the same run. For the reference cell, set up data acquisition for both interference optics and absorbance optics. The interference optics proceeds as usual with centering the acquisition angle to the middle of the sector, maximizing fringe contrast. The absorbance scan settings should specify a wavelength of 280 nm and acquisition radial step size of 0.001 cm across the range from 5.65 to 7.25 cm. An important deviation from standard protocol is the acquisition of intensity data instead of absorbance. This allows edges of transmission to be observed more accurately.

Step 3: Analysis of radial calibration factor.

The software MARC was written to process scans from fringe shift data of the Rayleigh interference optical system and the recorded intensity data from the absorbance optical system. Briefly, after loading a set of at least ten replicate scans acquired during the calibration run, the program identifies equivalent points on the edges of the lines and calculates the average pitch (i.e., spacing). Since the offset of patterns in sample and reference side is half the pitch, an apparent deviation from this shift arises from rotation of the mask. This allows the rotation angle to be calculated, and cosine errors to be factored into the analysis of the pitch. From the calibrated known pitch and the apparent pitch in the measured data, a correction factor R is calculated as the ratio of the two.

Sedimentation velocity experiment of reference molecule

In our experience, based on the multilaboratory benchmark study, bovine serum albumin (BSA) is a solid choice as a molecule that can be reproducibly used in many AUC experiments, with its hydrodynamically resolved monomer s -value as the key parameter for assessing the accuracy of the measurement. However, BSA is a commercially available material which can be found in various formulations. Additionally, the user has no information on the possible variation in different lots. This can potentially lead to variations in the exact s -value of BSA monomer. Recently, the NIST monoclonal antibody (NISTmAb) reference material, RM 8671, which is intended for use in evaluating the performance of different methods for physical–chemical properties, has become commercially available (Schiel et al. 2018). The standardized formulation and convenient availability lends itself well to be used as a reference material for AUC measurement.

Step 1 Prepare reference sample and assemble the reference sample cell.

If using BSA, dissolve 10 mg lyophilized powder in 1 mL phosphate-buffered saline (PBS) and dialyze overnight. Measure the BSA concentration spectrophotometrically and dilute into PBS to achieve a final concentration of ~ 0.5 mg/mL (or ~ 0.35 OD₂₈₀). If using NISTmAb, dilute in the formulation buffer [12 mM histidine pH 6.0 (Schiel et al. 2018)] to a final concentration of ~ 0.5 mg/mL (or ~ 0.7 OD₂₈₀).

Assemble a standard AUC sample cell with 12 mm optical pathlength centerpieces and sapphire windows. Load 400 μ L of protein solution and 400 μ L of the corresponding reference buffer in the sample and reference sector, respectively, and close both loading ports. It is highly desirable to

dedicate the cell components to the reference sample and keep the cell assembled in the refrigerator after the run. Sample may be resuspended by gentle mixing after the run (Schuck and Zhao 2020) and reused for subsequent calibration and quick diagnostic experiments.

Step 2 Carry out SV experiment with reference sample and calibration cell

Place the reference sample cell in the rotor opposite to the counterbalance, adjusting the latter to balance weight. Also insert into the same rotor the radial calibration cell described above, and its weight balancing extra cell. Carefully align all cells in the rotor. Place the rotor into the AUC chamber, install the optical arm, and pull the vacuum. After a rough vacuum is achieved, set a target temperature of 20 °C at the centrifuge console and a target rotor speed of 0 rpm, and start the run. In this state let the centrifuge temperature equilibrate for 2–3 h, or 2 h beyond the time when the temperature reading equals the set-point.

At the instrument computer, set up the experimental parameters to a rotor speed close to 50,000 rpm, 20 °C, acquiring interference data and absorbance data for both the radial magnification and the reference sample cell. For the radial magnification cell, use the scan settings outlined above. For the sample cell, set the data acquisition wavelength to 280 nm and scan with a step size of 0.003 cm from 6.0 to 7.23 cm in 1 min time intervals. Under the Options menu of the AUC control software, switch to absorbance data acquisition in intensity mode. When sufficient time for temperature equilibration has passed (above), initiate rotor acceleration, adjust interference optics exposure to the middle of the sectors, and commence scan data acquisition. The experiment can be stopped after several hours once the trailing edge of the protein sedimentation boundary has migrated outside the radial observation window.

Sedimentation velocity analysis and time correction

The measurement of the sedimentation time is conveniently on a scale that can be measured very precisely by common digital clocks. Therefore, it is bewildering that AUC scan files are in error in this parameter. Fortunately, the scan file metadata has a timestamp from the computer clock which is sufficiently precise to time the scan intervals. This information is automatically evaluated in the software SEDFIT and REDATE, and ASCII scan files are re-written to correct the nominal elapsed time since the start of the sedimentation in the file header.

The second kind of timing error is caused by the finite scan velocity of the absorbance system. For this, the scanning step size is important. This effect can be taken into account in the data analysis on the level of modeling the

recorded sedimentation process, or simply by a correction to the apparent s -value based on scanning range and velocity (Brown et al. 2009; Ghirlando et al. 2013; Schuck 2016), following

$$\frac{s}{s'} = \left[1 - \frac{s\omega^2(b-m)}{v_E \log(b/m)} \right] \quad (1)$$

with s' the apparent velocity, s the actual velocity, ω the rotor angular velocity, m and b the meniscus and bottom, respectively, and v_{scan} the scanner velocity (Brown et al. 2009). With the scan settings above (data interval 0.003 cm) the absorbance radial scan speed during rotor rotation at 50,000 rpm has been measured as 2.43 cm/min, which leads to an error in s -values by 0.18% for the BSA monomer and by 0.25% for the NISTmAb. [For 0.002- and 0.001-cm intervals and single acquisitions, the measured scan speeds were 1.65 and 0.94 cm/min, respectively, leading to slightly different scan velocity correction factors (Brown et al. 2009)]. Considering the magnitude of correction factors, it is sufficient to insert the apparent value s' in the right-hand side of Eq. (1).

Step 1: correct scan files for time errors.

Load the entire run data into the software REDATE to create copies of the scan files with corrected entries. The corrected scan files are recognized in SEDFIT as such, and no further time correction is applied. Alternatively, data can be loaded into SEDFIT directly, which will, by default, check the file timestamps and suggest creating copies of scan files with corrected entries. REDATE is more convenient in that it can correct data from the entire run at once. For the details of time correction, see (Zhao et al. 2013).

An important detail is in the creation of archives for data transfer between AUC and data analysis computer. Unless the time correction has occurred already, the archive must be created such that the file metadata is preserved. This is usually the case when archiving on the level of folders, as opposed to a set of scan files. Whether metadata in scan files are preserved can be easily inspected through examining file creation dates and times (Fig. 3). These should reflect the data acquisition, and not the time when the archive was expanded.

Step 2: calculate sedimentation coefficient distribution $c(s)$ for the reference sample.

Separately for absorbance and interference data, load the time-corrected scan files into SEDFIT, and calculate a standard $c(s)$ distribution (Schuck 2016) (Fig. 4). After integration of the monomer peak, record the weight-average s -values of the monomer, s_{app} , for each data set.

Step 3: apply correction factors to arrive at the corrected s -value

Proceeding as described above, the errors in recorded time are already accounted for, leaving the radial magnification and temperature (viscosity) errors, and, for the absorbance data the scan velocity error:

$$s_{\text{cal},20} = s_{\text{app}} \times R \times \left(\frac{\eta_{\text{true}C}}{\eta_{20}} \right) \times \left[1 - \delta_{\text{ABS/IF}} \times \frac{s_{\text{app}} \omega^2 (b-m)}{v_{\text{scan}} \log(b/m)} \right], \quad (2)$$

where we define the symbol $\delta_{\text{ABS/IF}}$ as 1 for absorbance data and 0 for interference data (such that the last term vanishes).

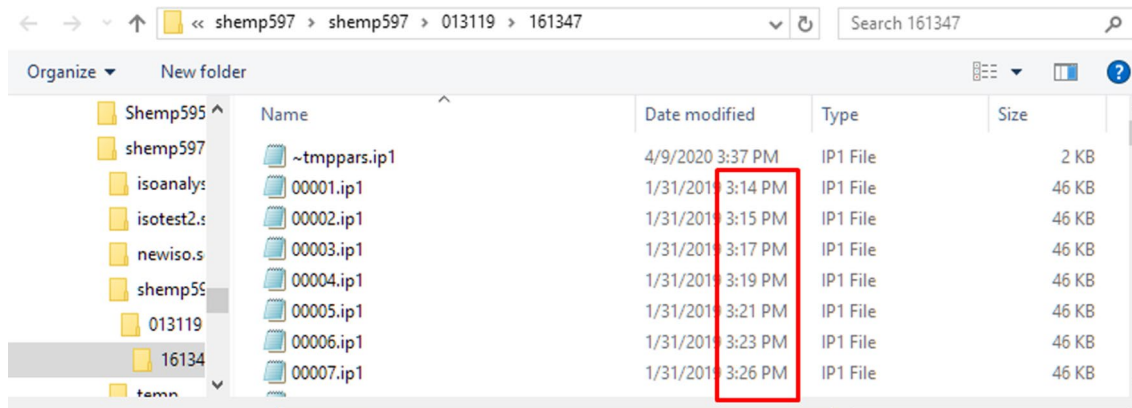


Fig. 3 Screenshot of AUC scan files in the Windows File Explorer displaying scan file time metadata (red highlight). The precision of the file creation times is greater than displayed, and more details may be visualized, for example, through exploring the individual file prop-

erties. File creation data are stored in seconds, which for a run of several hours provides a relative precision on the order of ~0.01%. For details see (Ghirlando et al. 2013; Zhao et al. 2013)

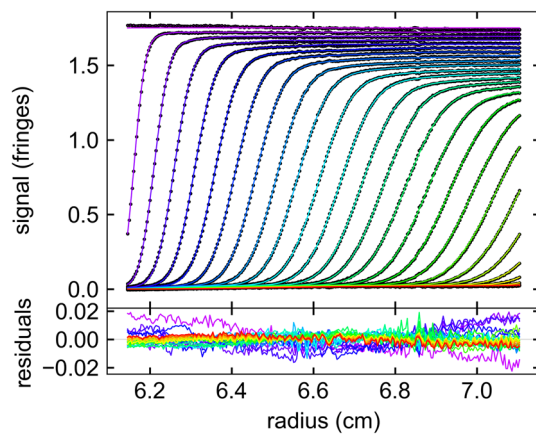


Fig. 4 Example of 0.5 mg/mL NISTmAb sedimenting at 48,000 rpm as recorded by Rayleigh interference optics. Shown are every 5th data point of consecutive scans (circles), and the best-fit $c(s)$ analysis model (lines) with residuals in the enhanced scale below. The resulting rmsd is 0.003543 fringes (0.21% of total signal). This plot and those of Figs. 5 and 6 were created using the software GUSSE (Brautigam 2015) (kindly provided by Dr. Chad Brautigam at utsouthwestern.edu/labs/mbr/software) which interfaces with SEDFIT

In case the temperature deviation is very large, additional density corrections may be applied (Ghirlando et al. 2013).

Results

Following the above protocol, we have carried out external calibration of three AUC instruments in our laboratory, each using absorbance and interference optical detection systems, and ‘pre-calibrated’ in radius according to manufacturer’s instructions. The external radial calibration was based on the steel mask (Ghirlando et al. 2013). For the reference SV experiment assessing the consistency of

calibration, we used NISTmAb. The run was carried out at a rotor speed of 48,000 rpm instead of the slightly more optimal 50,000 rpm, to prevent potential run failure due to scratches on the overspeed disk of the rotor used. For each instrument, we acquired NISTmAb data in duplicate by resuspending the sample after the calibration run and carrying out a replicate SV run.

Using the same set-point of 20 °C, the measured actual temperatures in the three instruments were 19.7, 20.1, and 21.6 °C, respectively. The radial correction factors for interference/absorbance detection were 1.014/1.012, 1.004/1.013, and 1.002/1.013, respectively (Table 1). The scan time errors under the present conditions were 0.14%.

For the twelve NISTmAb data sets, excellent fits were achieved throughout (Fig. 4), allowing discrimination of any trace dimers and higher aggregates and providing a clear determination of the monomer s -values. As may be discerned from the $c(s)$ distributions in Fig. 5 and the integrated monomer s -values in Table 1, these uncalibrated sedimentation velocities differ significantly among instrument and optical detection system, spreading across a range of 6.22–6.61 S, with a standard deviation of 0.15 S.

After application of the temperature, radial magnification, and scan velocity calibration factors to the s -values, the $c(s)$ distributions are better aligned, as shown in Fig. 6. The standard deviation of the corrected s -values is reduced to 0.014 S (less than one-tenth of the uncorrected value), with a best-estimate for the NISTmAb monomer of $6.349 \text{ S} \pm 0.004 \text{ S}$ (SEM). It should be noted this does not yet reflect values corrected to the water at 20 °C standard, but instead the values for buffer (in this case 5 mM histidine) at 20 °C. A more detailed graphical presentation of individual monomer s -values before and after calibration is shown in Fig. 7.

Table 1 Calibration factors and NISTmAb sedimentation coefficient

Instrument	Run # & detection	S_{exp} (S)	Temperature (°C)	Viscosity factor	Radial factor	Scan velocity factor	Calibrated s -value (S)
Curly	1 ABS	6.219	19.7029	1.0073	1.0144	0.9975	6.339
	1 IF	6.238	19.7029	1.0073	1.0122	1	6.360
	2 ABS	6.219	19.7029	1.0073	1.0144	0.9975	6.339
	2 IF	6.231	19.7029	1.0073	1.0122	1	6.353
Larry	1 ABS	6.346	20.1400	0.99659	1.0044	0.9975	6.336
	1 IF	6.297	20.1400	0.99659	1.0127	1	6.355
	2 ABS	6.341	20.1400	0.99659	1.0044	0.9975	6.331
	2 IF	6.323	20.1400	0.99659	1.0127	1	6.381
Shemp	1 ABS	6.598	21.6382	0.96119	1.0017	0.9975	6.337
	1 IF	6.519	21.6382	0.96119	1.0130	1	6.348
	2 ABS	6.612	21.6382	0.96119	1.0017	0.9975	6.350
	2 IF	6.53	21.6382	0.96119	1.0130	1	6.358

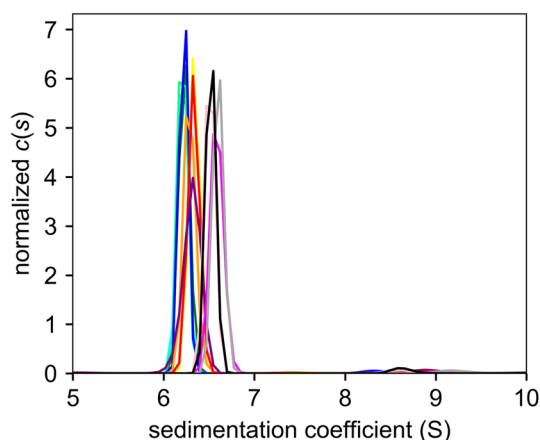


Fig. 5 Uncalibrated measured $c(s)$ distributions of 0.5 mg/mL NISTmAb in three different instruments, two different optical detection systems, acquired in replicate (12 data sets total, plotted in different colors). For details on integrated monomer s_w -values and precise run, information see Table 1

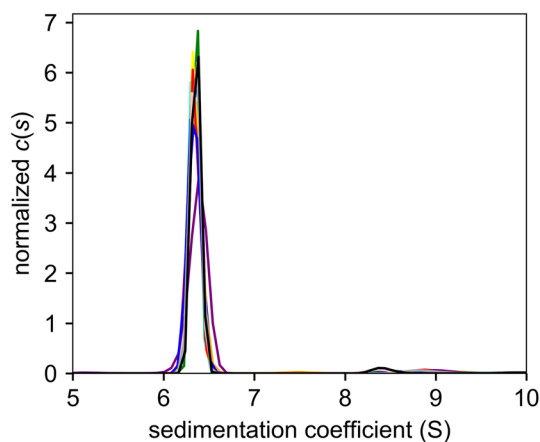


Fig. 6 $c(s)$ distributions of NISTmAb after application of calibration corrections for the same data sets shown in Fig. 5. For details on numerical values see Table 1

Discussion

A major virtue of AUC is that it is an absolute method grounded in first principles, but this is only true if the data dimensions can be trusted and the instrument is properly calibrated. Some classes of experiments, such as quantitation of trace aggregates in the pharmaceutical industry, or the measurement of binding constants in concentration series, may be carried out in a ‘relative mode’, but even these will usually require experimental reproducibility from instrument to instrument and from one month to the next. For many aspects of AUC that we take for granted, the absolute values are crucial, for example, roughly

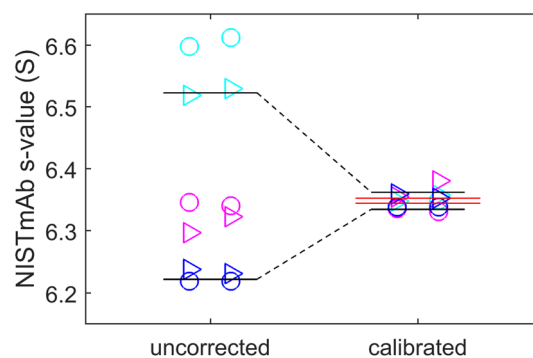


Fig. 7 Measured uncorrected and calibrated monomer s -value of NISTmAb monomer for instruments Shemp (cyan), Larry (magenta), and Curly (blue) in absorbance (circles) and interference (triangles) detection, each in two consecutive runs (horizontal offset). The black horizontal lines are mean \pm standard deviation, and the red horizontal lines depict the mean \pm standard error of the mean. For individual values see Table 1

estimating protein molecular weights from s -values, or even more so for comparison of hydrodynamic shapes with data from small angle scattering or theoretical hydrodynamic calculations (García de la Torre et al. 2000; Rai et al. 2005; Aragon 2011; Perkins et al. 2011). The motivation of the present protocol was to provide a review of calibration procedures and magnitude of systematic errors and to demonstrate the utility of the NISTmAb reference molecule (Schiel et al. 2018) as a standard in AUC calibration.

The recent discovery of time-errors on the order of 10% on all instruments (Zhao et al. 2013; The Editors 2013), and the discovery of significant systematic errors in other measurements in many instruments in a large multilaboratory study (Zhao et al. 2015), show the magnitude of the problem. In the absence of any control measurements or calibrations, s -values spanning a range of $\pm 15\%$ were observed for the same BSA monomer sample, with a standard deviation of 4.4%. This is consistent with the uncorrected results in the present study using three instruments in our laboratory with NISTmAb as control. Regarding the present NISTmAb results, it should be noted that all instruments receive regular manufacturer maintenance and appear fully functioning and that their performance characteristics are highly stable over time.

The largest sources of errors are found in rotor temperature, radial magnification, and—surprisingly—time measurements. The absolute radius position has a secondary impact, as shown in a detailed analysis of the multilaboratory data (Zhao et al. 2015). In this regard, recently, a strategy for determining the absolute positions of the bottom of the solution column was proposed by Stoutjesdyk et al. (2020), but we think this is usually of no or secondary concern in SV, and must be considered a fitting parameter in sedimentation equilibrium analysis if using soft mass

conservation constraints in the analysis (Vistica et al. 2004; Brown and Schuck 2008).

Fortunately, the previous multilaboratory study has demonstrated (Zhao et al. 2015) that, if we apply critical calibration procedures for time, temperature, and radial magnification, these jointly improve the accuracy significantly. Similarly, the data from the present study show an order of magnitude improvement in precision across instruments in our laboratory when using the NISTmAb as a control. This molecule has potentially significant advantages for use as a control by avoiding uncontrolled vendor- or lot-dependent variation. In the current study, we have observed that the same NISTmAb sample can be resuspended and used for multiple experiments, which offers an additional benefit for the calibration experiments. Regarding the time correction, unfortunately, the independent scan time measurement has been disabled by the manufacturer's design of the newest AUC model (Beckman Coulter Optima AUC), which strips the scan files of their metadata that enable error detection. It is our hope that this will be changed in the future.

Finally, we note that the procedure for radial magnification measurement using a NIST calibrated reference window will be equally applicable to other optical systems for AUC that are currently being developed in different laboratories (Strauss et al. 2008; Pearson et al. 2017; Wawra et al. 2019). More generally, the calibration efforts described here are synergistic to improvements in the precision of SV through the development of cell alignment tools (Gabrielson et al. 2009; Doyle et al. 2017, 2020; Channell et al. 2018), which should also prove universally useful in AUC.

Acknowledgements This work was supported by the Intramural Research Program of the National Institute of Biomedical Imaging and Bioengineering, National Institutes of Health.

Funding National Institutes of Health, ZIA EB00051-14 LCIM.

Code availability Compiled software *SEDFIT* for scan time correction and sedimentation velocity data analysis and *MARC* for radial calibration will be freely available for download at sedfitsedphat.nibib.nih.gov/software.

Compliance with ethical standards

Conflict of interest There are no conflicts of interest.

References

- Aragon SR (2011) Recent advances in macromolecular hydrodynamic modeling. *Methods* 54:101–114. <https://doi.org/10.1016/j.ymeth.2010.10.005>
- Brautigam CA (2015) Calculations and publication-quality illustrations for analytical ultracentrifugation data. *Methods Enzymol* 562:109–133. <https://doi.org/10.1016/bs.mie.2015.05.001>
- Brown PH, Schuck P (2008) A new adaptive grid-size algorithm for the simulation of sedimentation velocity profiles in analytical ultracentrifugation. *Comput Phys Commun* 178:105–120. <https://doi.org/10.1016/j.cpc.2007.08.012>
- Brown PH, Balbo A, Schuck P (2009) On the analysis of sedimentation velocity in the study of protein complexes. *Eur Biophys J* 38:1079–1099. <https://doi.org/10.1007/s00249-009-0514-1>
- Cecil R, Ogston AG (1948) The accuracy of the Svedberg oil-turbine ultracentrifuge. *Biochem J* 43:592–598. <https://doi.org/10.1042/bj0430592>
- Channell G, Dinu V, Adams GG, Harding SE (2018) A simple cell-alignment protocol for sedimentation velocity analytical ultracentrifugation to complement mechanical and optical alignment procedures. *Eur Biophys J* 1:3. <https://doi.org/10.1007/s00249-018-1328-9>
- Doyle BL, Budyak IL, Rauk AP, Weiss WF (2017) An optical alignment system improves precision of soluble aggregate quantitation by sedimentation velocity analytical ultracentrifugation. *Anal Biochem*. <https://doi.org/10.1016/j.ab.2017.05.018>
- Doyle BL, Rauk AP, Weiss WF, Budyak IL (2020) Quantitation of soluble aggregates by sedimentation velocity analytical ultracentrifugation using an optical alignment system—aspects of method validation. *Anal Biochem*. <https://doi.org/10.1016/j.ab.2020.113837>
- Errington N, Rowe AJ (2003) Probing conformation and conformational change in proteins is optimally undertaken in relative mode. *Eur Biophys J* 32:511–517. <https://doi.org/10.1007/s00249-003-0315-x>
- Gabrielson JP, Arthur KK, Stoner MR et al (2009) Precision of protein aggregation measurements by sedimentation velocity analytical ultracentrifugation in biopharmaceutical applications. *Anal Biochem* 396:231–241. <https://doi.org/10.1016/j.ab.2009.09.036>
- García de la Torre J, Huertas ML, Carrasco B (2000) Calculation of hydrodynamic properties of globular proteins from their atomic-level structure. *Biophys J* 78:719–730. [https://doi.org/10.1016/S0006-3495\(00\)76630-6](https://doi.org/10.1016/S0006-3495(00)76630-6)
- Ghirlando R, Balbo A, Piszczek G et al (2013) Improving the thermal, radial, and temporal accuracy of the analytical ultracentrifuge through external references. *Anal Biochem* 440:81–95. <https://doi.org/10.1016/j.ab.2013.05.011>
- Ghirlando R, Zhao H, Balbo A et al (2014) Measurement of the temperature of the resting rotor in analytical ultracentrifugation. *Anal Biochem* 458:37–39. <https://doi.org/10.1016/j.ab.2014.04.029>
- Harding SE, Rowe AJ (2010) Insight into protein-protein interactions from analytical ultracentrifugation. *Biochem Soc Trans* 38:901–907. <https://doi.org/10.1042/BST0380901>
- LeBrun T, Schuck P, Wei R et al (2018) A radial calibration window for analytical ultracentrifugation. *PLoS ONE* 13:e0201529. <https://doi.org/10.1371/journal.pone.0201529>
- Pearson J, Walter J, Peukert W, Cölfen H (2017) Advanced multiwavelength detection in analytical ultracentrifugation. *Anal Chem*. <https://doi.org/10.1021/acs.analchem.7b04056>
- Perkins SJ, Nan R, Li K et al (2011) Analytical ultracentrifugation combined with X-ray and neutron scattering: experiment and modelling. *Methods* 54:181–199. <https://doi.org/10.1016/j.ymeth.2011.01.004>
- Rai N, Nöllmann M, Spotorno B et al (2005) SOMO (Solution MOdeler) differences between X-Ray- and NMR-derived bead models suggest a role for side chain flexibility in protein hydrodynamics. *Structure* 13:723–734. <https://doi.org/10.1016/j.str.2005.02.012>
- Schiel JE, Turner A, Mouchahoir T et al (2018) The NISTmAb reference material 8671 value assignment, homogeneity, and stability. *Anal Bioanal Chem* 410:2127–2139. <https://doi.org/10.1007/s00216-017-0800-1>
- Schuck P (2013) Analytical ultracentrifugation as a tool for studying protein interactions. *Biophys Rev* 5:159–171. <https://doi.org/10.1007/s12551-013-0106-2>

- Schuck P (2016) Sedimentation velocity analytical ultracentrifugation: discrete species and size-distributions of macromolecules and particles. CRC Press, Boca Raton
- Schuck P, Zhao H (2017) Sedimentation velocity analytical ultracentrifugation: interacting systems. CRC Press, Boca Raton
- Schuck LM, Zhao H (2020) Resuspending samples in analytical ultracentrifugation. *Anal Biochem* 604:113771. <https://doi.org/10.1016/j.ab.2020.113771>
- Schuck P, Zhao H, Brautigam CA, Ghirlando R (2015) Basic principles of analytical ultracentrifugation. CRC Press, Boca Raton
- Stoutjesdyk M, Henrickson A, Minors G, Demeler B (2020) A calibration disk for the correction of radial errors from chromatic aberration and rotor stretch in the Optima AUCTM analytical ultracentrifuge. *Eur Biophys J*. <https://doi.org/10.1007/s00249-020-01434-z>
- Strauss HM, Karabudak E, Bhattacharyya S et al (2008) Performance of a fast fiber based UV/Vis multiwavelength detector for the analytical ultracentrifuge. *Colloid Polym Sci* 286:121–128. <https://doi.org/10.1007/s00396-007-1815-5>
- Svedberg T, Pedersen KO (1940) The ultracentrifuge. Oxford University Press, London
- The Editors (2013) Editorial: recorded scan times can limit the accuracy of sedimentation coefficients in analytical ultracentrifugation. *Anal Biochem* 437:103. <https://doi.org/10.1016/j.ab.2013.02.017>
- Vistica J, Dam J, Balbo A et al (2004) Sedimentation equilibrium analysis of protein interactions with global implicit mass conservation constraints and systematic noise decomposition. *Anal Biochem* 326:234–256. <https://doi.org/10.1016/j.ab.2003.12.014>
- Wawra SE, Onishchukov G, Maranska M et al (2019) A multiwavelength emission detector for analytical ultracentrifugation. *Nanoscale Adv* 1:1387–1394. <https://doi.org/10.1039/C9NA00487D>
- Zhao H, Ghirlando R, Piszczek G et al (2013) Recorded scan times can limit the accuracy of sedimentation coefficients in analytical ultracentrifugation. *Anal Biochem* 437:104–108. <https://doi.org/10.1016/j.ab.2013.02.011>
- Zhao H, Balbo A, Metger H et al (2014) Improved measurement of the rotor temperature in analytical ultracentrifugation. *Anal Biochem* 451:69–75. <https://doi.org/10.1016/j.ab.2014.02.006>
- Zhao H, Ghirlando R, Alfonso C et al (2015) A multilaboratory comparison of calibration accuracy and the performance of external references in analytical ultracentrifugation. *PLoS ONE* 10:e0126420. <https://doi.org/10.1371/journal.pone.0126420>
- Zhao H, Li W, Chu W et al (2020) Quantitative analysis of protein self-association by sedimentation velocity. *Curr Protoc Protein Sci* 101:1–15. <https://doi.org/10.1002/cpps.109>

Publisher's Note Springer Nature remains neutral with regard to jurisdictional claims in published maps and institutional affiliations.